Groundwater Vulnerability and Risk Mapping Based on Residence Time Distributions: Spatial Analysis for the Estimation of Lumped Parameters

Myriam Dedewanou, Stéphane Binet, Jean-Louis Rouet, Yves Coquet, Ary Bruand, Hervé Noel

Groundwater vulnerability and risk mapping based on Residence Time Distributions: Spatial analysis for the estimation of lumped parameters

M. Dedewanou [1,2], S. Binet [1, 3], JL. Rouet[1], Y. Coquet[1], A. Bruand[1], H. Noel[2]

[1] ISTO, UMR 7327 CNRS-Université d'Orléans-BRGM, 45071 Orléans cedex 2

[2] GEO-HYD, 101 rue Jacques Charles, 45160, Olivet, France.

[3] ECOLAB, UMR 5245 CNRS-UPS-INPT, 31326 Castanet-Tolosan, France

---

Abstract

Specific vulnerability estimations for groundwater resources are usually geographic information system-based (GIS) methods that establish spatial qualitative indexes which determine the sensitivity to infiltration of surface contaminants, but with little validation of the working hypothesis. On the other hand, lumped parameter models, such as the Residence Time Distribution (RTD), are used to predict temporal water quality changes in drinking water supply, but the lumped parameters do not incorporate the spatial variability of the land cover and use. At the interface between these two approaches, a GIS tool was developed to estimate the lumped parameters from the vulnerability mapping dataset. In this method the temporal evolution of groundwater quality is linked to the vulnerability concept on the basis of equivalent lumped parameters that account for the spatially distributed hydrodynamic characteristics of the overall unsaturated and saturated flow nets feeding the drinking water supply. This vulnerability mapping method can be validated by field observations of water concentrations. A test for atrazine specific vulnerability of the Val d'Orléans karstic aquifer demonstrates the reliability of this approach for groundwater contamination assessment.

Keywords: Specific vulnerability, advection / dispersion, residence time distribution, equivalent parameters.

1. Introduction

The main tools for the management and the conservation of groundwater resources consist in characterizing the vulnerability of the aquifer used for drinking water. Intrinsic vulnerability uses physical characteristics as criteria to determine the sensitivity of groundwater to surface pollution. Most intrinsic vulnerability maps are multi-criteria, weighted and index-based, developed by Aller et al., (1987), Doerfliger et al., (1999), Petelet-Giraud et al., (2001) and Civita and De Maio (2004). The specific vulnerability of groundwater incorporates the physico-chemical properties and their relationship with the natural environment as supplementary criteria in the vulnerability index estimation (Vrba and Zaporozec, 1994). These tools enable policies for the development of codes of practice for groundwater protection to be proposed (Escolero et al. 2002) and open up significant opportunities to enhance the efficacy of water vulnerability assessment tools by incorporating indicators and operational measures for social considerations (Plummer et al., 2012). While the area of use is huge, the index calculation method is limited because the weighting is usually arbitrarily chosen. These approaches are qualitative and highly subject to the hydrogeologist's interpretation (Panagopoulos et al., 2006).

Borehole vulnerability analysis was developed for drinking water supplying watersheds. This method completes the vulnerability index with the notions of distance, horizontal flow rate and transport to the target (borehole or spring) (Goldscheider and Popescu, 2003). In this framework, two types of vulnerability can be defined: a resource vulnerability which only takes vertical transfer into account, and a borehole vulnerability which incorporates the horizontal transfer into the borehole. The key parameters for the evaluation of specific vulnerability are the residence time of contaminants, their capacity of migration underground and the

attenuation process. Some authors (Neukum et al., 2008; Anderson and Gosk 1987; Sadek and Abd El-Samie, 2001; Bakalowicz, 2005) suggested that a high vulnerability is related to a short residence time of the main part of the recharge. From these concepts, Brouyère (2001) relate a potential contamination to the transfer time, concentration level and duration of the phenomenon, plotted along the three axe of the cube. Jeannin et al. (2001) developed a program that relates field observations to concentration level, transfer time and duration. The model assumes an instantaneous release of a conservative contaminant at a given point on the land surface and simulates the resulting breakthrough curves at the outlet of each sub-system by means of the advection - dispersion equation, disregarding retardation and degradation processes (Zwahlen, 2003).

By linking the vulnerability index to physical parameters, the working hypothesis used in vulnerability mapping can be tested. Goldscheider et al. (2001) released different tracers at the land surface and observed the breakthrough at a target (spring), the travel time, the concentration and the tracer recovery rate to validate a vulnerability map. Holman et al. (2005) validated an intrinsic groundwater vulnerability method using a national nitrate database and some co-variance and variance analyses. Neukum et al. (2008) worked on the validation of a vulnerability map based on field investigation and column tracer experiments conducted on soil materials. The authors modelled tracer displacements using the advection – dispersion model and proposed a transit time distribution function of the tracer that depends on the geometric and hydraulic boundary conditions of the aquifer. Lasserre et al. (1999) developed a simple GIS-linked model to describe the groundwater transport of nitrates. For all these methods, developed to validate vulnerability criteria, the aim was to link surface land use with watershed hydrodynamic properties and water quality at the boreholes.

For time series analysis, several studies have applied an impulse response at the watershed scale for solute transport modeling purposes (Jury, 1982; Beltman et al., 1994; Barry and Parker, 1987; Molénat et al., 1999; Schwientek et al., 2009). The method consists in establishing a residence time distribution (RTD) to link pollutants at the surface of the

watershed to the contaminant concentrations measured in the borehole. Related to the geometry of the aquifer, Jurgens et al., (2012) proposed six theoretical models, (derived from analytical solutions of the advection - dispersion reaction equation) to fit the impulse response with three lumped parameters. These parameters vary from one study to another, but the ones most widely used are the average residence time, the Peclet number and the rate of degradation. To evaluate groundwater quality trends, Visser et al. (2009) after a comparison between statistical, groundwater dating and deterministic modeling, showed that impulse response methods require little information about the physical system, but rather rely on the available data, which makes them suitable for application to a wide variety of systems.

Linking the spatial properties that determine the vulnerability and the temporal evolution of the water quality is a key point for water resource management. At the watershed scale, some semi-distributed models incorporate the soil surface properties to model water quality with a GIS dataset based on an impulse response, such as the SWAT model (Srinivasan and Arnold, 1994) or on a flow model such as Drainmod (Fernandez *et al.* 2006) MACRO (Larsbo and Jarvis, 2003) and STICS (Ledoux, 2003). For groundwater quality purposes, the flow paths must be analyzed in 3 dimensions but few tools are available to compute an impulse response from the spatially distributed 3D groundwater properties.

This paper proposes a method to calculate a RTD impulse response in aquifers based on spatial datasets used for specific vulnerability assessments. The spatial GIS vulnerability dataset corresponds to the thickness and hydrodynamic parameters of the geological formations found along the groundwater flow nets.

Based on the impulse response, which is characteristic of the watershed, the vulnerability index is defined as the mass ratio between the contaminants that exceeds a fixed threshold at the borehole and the injected mass. This makes it possible to map the relative vulnerability of each infiltration surface where contaminant application occurs. This approach includes residence times, dispersion and attenuation. Spatial vulnerability mapping is validated with GIS using the temporal evolution of the groundwater quality.

2. The Residence Time Distribution (RTD)

The Residence Time Distribution (RTD) is a probability distribution function that describes the amount of time a fluid element can spend inside the column. After a pulse of mass M, its RTD is defined as :

$$E(t) = \frac{Q\,C(t)}{M} = \frac{M\,(t)}{M} \quad \textit{(Equation 1)}$$

Here Q [$L^3.T^{-1}$] is the discharge flowing through the column.

The concentration *C(t)* [$M.L^{-3}$] can be obtained by solving the transport equation along a column open at both ends (Kreft and Zuber, 1978). For the transport of a pulse of mass M in a porous one-dimensional column (the transversal section is A [L^2], the length x and the column water content is θ), where water flow with a velocy (u) there is many analytical solutions, most of them use the non-dimensional Peclet number (Pe*)*, the average residence time ($\bar{t}$) and the rate of degradation λ [T^{-1}] of the contaminant during transport.

To assume that the column is open at both ends (Levenspiel 1962, Maloszewski and Zuber, 1982) enables to express the RTD as follow:

$$E(t) = \sqrt{\frac{Pe}{4\pi t\bar{t}}} \exp\left[-\frac{Pe\,(\bar{t}-t)^2}{4t\bar{t}}\right] \exp\left[-\lambda\, t\right] \quad \textit{(Equation 2)}$$

The contaminant transport through the column is described with only three parameters and no assumption is made on the laminar, turbulent, unsaturated or saturated nature of the flows. Degradation and delay are taken into account with λ and $\bar{t}$. If no reaction occurs, $\bar{t}$ is the same as the average residence time of the water in the column.

2.1. RTD for a column with multi layers.

For the transport of a pulse, the mean residence time $\bar{t}$ [T] of the contaminant in the column can be defined either with the $C(t)$ curve or as the ratio between the water flux (u) and the stored water (θ L):

$$\bar{t} = \frac{\int_0^\infty t\, C(t)\, dt}{\int_0^\infty C(t) dt} = \frac{u}{\theta\, L} \quad \textit{(Equation 3)}$$

Another important descriptor of the $C(t)$ curve is its variance:

$$\sigma^2 = \frac{\int_0^\infty (t-\bar{t})^2\, C(t)\, dt}{\int_0^\infty C(t) dt} \quad \textit{(Equation 4)}$$

In decomposing the borehole watershed into *n* parallel flow nets. This reduces the non-linear three-dimensional problem to a linear one-dimensional one. The water and the contaminant mass which infiltrate the ground enter through the various i layers of the aquifer where the hydro-dispersive properties can vary. They flow through the i layers until the borehole, following the flow nets. For every n flow net, the i layers are considered to be independent columns characterized by the average residence time $\bar{t}_{n,i}$ and the Peclet number $Pe_{n,i}$.

For i serial layers, equivalent properties can be calculated. The mean residence time for the n^{th} flow net, where contaminant flows through i serial columns, is:

$$\langle \bar{t}_n \rangle = \sum_1^i \bar{t}_{n,i} \quad \textit{(Equation 5)}$$

In 1959, Aris showed that, in the case of an infinite column, the change in the variance (equation 4) between two points can be described as:

$$\frac{\Delta\sigma^2}{\bar{t}^2} = \frac{2}{Pe} \quad \textit{(Equation 6)}$$

Thus, if this relation is extended to i serial columns, the equivalent Peclet number <Pe_n> for the n^{th} flow net, can be defined as:

$$\frac{\langle Pe_n \rangle}{2} = \frac{\langle \bar{t}_n^2 \rangle}{\Delta\sigma^2_{n,i} \text{-} \ldots \text{-} \Delta\sigma^2_{n,1}} = \frac{\langle \bar{t}_n^2 \rangle}{\sum_1^i \left(\frac{2\bar{t}_{n,i}^2}{Pe_{n,i}} \right)} \quad \textit{(Equation 7)}$$

This formulation enables the residence time distribution $E_{n(t)}$ at the output of the n^{th} flow net to be described, using an equivalent average residence time and an equivalent Peclet number.

The mass of contaminant at the borehole is the sum of the mass arriving through the n flow nets. The RTD becomes:

$$E_{(t)} = \frac{\sum_1^n [E_{n(t)}\, M_n]}{\sum_1^n M_n} \textit{ (Equation 8)}$$

2.2. Computation of the equivalent lumped parameters using GIS

2.2.1. Water and contaminant fluxes at the upper boundary

The mass of contaminants entering the aquifer is considered to be the mass M [M] flowing under the organic soil zone. Published data on the rate of contaminant seeping under the soil (a) [/] compared to the initial pulverized mass M_0 can be used:

$$M = M_0 * a \text{ (Equation 9)}$$

The delay between pulverization and exportation under the roots in the soil is considered to be very small with respect to the average residence time used to describe groundwater flows.

2.2.2. Calculation of average residence times and Peclet numbers

First, the surface watershed of the borehole is discretized into unitary surfaces. The aquifer volume is divided into an unsaturated zone with vertical flows, and a saturated zone with horizontal flows. The contaminants flow first vertically toward the unsaturated zone, and then horizontally towards the borehole. Based on the groundwater head maps, the flow direction and the flow length (L) was defined for each of the n flow nets of the system. The calculation was carried out with the GIS ARCGIS® toolbox. For the unsaturated zone, the flow length L is simply calculated by the difference between the topographic and water head level.

Along each flow net, i columns can be discretized based on the 3D geological dataset. For each flow net n and i column, the equivalent Peclet number and the average residence time can be computed from with the hydrogeological dataset u, D, θ.

The equivalent parameters can be estimated using the GIS tool before being injected into the RTD equation (Equation 8).

2.3. Simulation of water quality by convolution

If we consider the various periods of infiltration as a sum of brief injections of mass M entering the column at time t', the concentration in the borehole $C_{(t)}$ can be deduced from the RTD:

$$C_{(t)} = \frac{1}{Q}\int_{-\infty}^{t} M_{t'} E_{(t-t')} e^{-\lambda (t-t')} dt' \quad \textit{(Equation 10)}$$

The history of the dissolved masses injected in the watershed (M) and the steady state average discharge of water across the borehole (Q) must be implemented. The Nash-Sutcliffe coefficient E (Nash and Sutcliffe, 1970) was used to assess the efficiency of the RTD model using equivalent parameters.

2.4. Analogy between RTD, vulnerability and risk indexes

The equivalent RTD for each flow net represents the mass arriving at the borehole for an injected mass equal to 1. Depending on the value of the equivalent parameters, and on the discharge Q_n for the n^{th} flow net, the concentrations obtained make it possible to identify flow nets showing concentrations higher than a threshold (LR) represented by the dashed line in Fig. 1 while other flow nets present concentrations below the threshold. The spatialized grid of equivalent parameters locates the surfaces which contribute to the over-concentration measured at the groundwater borehole, making it possible to prioritize the various surfaces in terms of borehole vulnerability and/or risk.

Using datasets of M values, the specific risk index *(I)* is defined as the rate between the mass above the threshold M_d (Fig. 1) and the mass flowing under the roots M. (equation 16).

$$I = \frac{M_d}{M} = \frac{\int_a^b [\frac{E(t)\,M}{Q_n} - LR]dt}{M} \quad \textit{(Equation 11)}$$

The boundaries a and b are defined in Fig 1 as the intercepts between the $C(t)$ curve and the fixed threshold. So, the specific risk index I is defined as the percentage of the applied contaminant mass which will reach the borehole above a given threshold. If M=1 for the entire watershed and the threshold has a low value, then equation 11 becomes an intrinsic vulnerability index.

3. Study site and data

The proposed model was tested on the Val d'Orléans karstic system, which has a wide range of flow velocities. This section presents the dataset required to apply the proposed methodology, and the various existing ways to compile this database.

3.1. The Val d'Orléans

The Val d'Orléans is located southeast of Orléans city, in the alluvial plain of the Loire river which corresponds to a depression of the main river bed. The length of this alluvial plain is about 40 km and its maximum width reaches 7 km in its central part (Fig. 2).

3.1.1. Pedology

Inside the protection zone (Fig.2A), clays In soil represent about 0 to 250 g/kg. The sand contents in silt (100 to 250 g/kg) and organic carbon (0 to 10 g/kg) are quite homogeneous (BDAT-GISSOL-INRA, 2014). This database shows a low content of clays and sands in the center and east of the perimeter and higher contents in the west zone. The values range respectively from 0 to 100 g/kg and from 100 to 250 g/kg.

3.1.2. Geology

The geology in this sector results from a major and regular marine sedimentation (transgression and regression phenomena), that started during the Trias and lasted until the beginning of the Tertiary (Eocene). White chalk with flint and detritical formations constitute the base of the geological formations of the Val d'Orléans. In the middle of the Tertiary (Oligocene, Aquitanien), a sedimentation of lacustrine origin formed the limestones of Beauce, interrupted with marly formations. In the second part of the Tertiary (Burdigalien), marls and sands were deposited, before being covered by fluvial (Quaternary) alluviums of the Loire (Auterives et al. 2014). For this study, only the sedimentary formations of lacustrine origin

229 which began during the Oligocene were of interest because it is the main aquifer. A karstic
230 network developed in the Beauce limestones, generally captive, either under the alluvial
231 formation or under the Burdigalien marls. A probability map of the karstic network was
232 proposed by Auterives et al., 2014.
233 This karstic network is supplied by surface water coming from the Loire river which infiltrates
234 at point sources (Albéric, 2004) in the area of Jargeau (Fig.2A) and by diffuse infiltration
235 through the alluvial plain located mainly in the river bed. Some of these karstic conduits outflow
236 downstream the Val d'Orléans where springs contribute to the establishment of the Loiret river
237 (Lepiller, 2006). Three drinking water boreholes are located within or close to the karstic
238 network (Fig. 2A). Based on the water quality data (isotopes and major elements) of the Loire
239 water, the local surface waters and the Loiret spring waters, Joigneaux (2011) revealed that
240 80% of the Loiret spring waters are composed of Loire water, the remainder being local surface
241 waters. Mixing is controlled by the hydrological conditions of the Loire river.
242 The groundwater vulnerability to diffuse agricultural pollution was estimated in the protection
243 zone of the three boreholes (Fig.2A).
244

245 ### 3.1.3. Water flux and contaminants below the root zone

246 The discharge values Q arise from the hydrological balance. This assessment was made by
247 various authors such as Chéry (1983), Livrozet (1984), Lepiller (2006), Lelong and Jozja
248 (2008), Gutierrez and Binet (2010). Three different flow values were considered according to
249 three hydrological scenarios. These three scenarios represent the minimal, maximal and
250 average flows that transit through the system. The minimal flow can be estimated from the
251 lowest contribution of the flow from the Loire river and the lowest contribution of impluvium in
252 the total hydrological balance assessment. The minimal value of the contribution of the river
253 Loire loss was estimated at 5 m^3/s (Martin and Noyer, 2003; Gutierrez and Binet, 2010),
254 whereas the lowest flow from the impluvium calculated by MACRO (Larsbo and Jarvis, 2003)

and calibrated for the Val d'Orleans is 0.100 m/year (Footways/Geo-Hyd, 2013). Thus, the minimal contribution in water supplied to the system was estimated at 186.10^6 m^3/year. 15% of the water comes from diffuse infiltration.

Concerning the average flow, the volume of the Loire loss to the Val d'Orléans aquifer, for an average year, was estimated by hydrological balance at 363.10^6 m^3/year. The results of models that estimate the effective rain, stemming from the impluvium, suggested a flow of 0.191 m/year (Joigneaux et al., 2011). The average flow transiting through the system is estimated to be 423.10^6 m^3/year. Here again, 15% of the water comes from diffuse infiltration. The proposed RTD model was tested and calibrated for the application of atrazine, which was sprayed between 1960 and 2003 on the maize crops. The reason for this choice is the quantitative availability of analyses done on the three Val d'Orléans boreholes, which revealed the presence of atrazine from the 1990s to 2004, showing, with a quarterly sampling frequency, an erratic response with values ranging from 0 to 0.3 µg/L. Atrazine concentration in the Loire river has been below the detection limit since the beginning of the century. In the 1990s, concentrations reached 0.3 µg/L (Joigneaux, 2011). It is considered that the totality of the atrazine concentration analysed at the three Val d'Orléans boreholes comes from diffuse infiltration through the alluvial plain. The Loire river dilutes the fluxes.

The localization of the maize crops was mapped in 2010 and was assumed to be constant through time (Fig. 2A). The atrazine masses injected during more than 40 years were estimated from the history of agricultural practices recorded in various ways, such as questionnaires collected by agricultural associations. Atrazine was applied by spraying, generally made once a year, in April. The quantities of atrazine applied decreased over time, (2.5 kg/ha/year in the 70^{th}, 1.5 in the 80^{th}, 1 betwwen 1991 to 1998, 0.75 in 1999 and 2000 and 0.5 betwwen 2000 to 2003) due to increasing constraints on the use of this herbicide, until it was banned in 2003. Some studies show that pesticides such as atrazine can have an export percentage up to 4 to 207 5% (Flury, 1996). Naturally, these ranges of values vary according

281 to the geo-hydro- morphological context of the site, but are mostly between 0.1 to 3%
282 (Wauchope, 1978; Flury, 1996; Voltz and Louchart, 2001).
283

284 3.2. Field data for RTD estimation

285 Establishing the RTD requires data concerning the hydrodynamic characteristics of the aquifer
286 (Table 1). Each hydrodynamic parameter is attributed to each surface of the grid area (250 m
287 by 250 m, Fig. 2A).
288 The hydrodynamic characteristics of the unsaturated zone (UZ) were attributed according to
289 the lithology of the four profiles already defined (sand (SD), sand and limestone (SD/LM), sand
290 and clay (SD/CL) and clay and sand (CL/SD)). The length of flows are known from the
291 topographic elevation nimus the aquifer water head (Desprez in 1967).
292 In the saturated zone (Table 1), 2000 borehole logs were analysed. Alluvium, limestone and
293 karstified limestones were observed in the area (Auterives et al. 2014). In a saturated context,
294 the water content is equal to the porosity.

295 3.2.3. Atrazine in groundwater

296 Estimating the specific vulnerability requires knowledge of the specific behaviour of the studied
297 contaminants. For atrazine, a 10-year database is available, with more than 110
298 measurements. The atrazine degradation rate is known to be 0.4 [month^{-1}] (IUPAC, 2013) and
299 rate of infiltration (a) was estimated at about 0.05 (Kladivko et al., 1991).
300

301 3.3. Parametric tests on the "Val d'orléans" dataset

302 Uncertainty on the parameterization was explored by calculating various RTDs to assess the
303 impact of parameterization on the results. Before estimating the vulnerability mapping with the
304 RTD model, various parameter values were tested to observe the variability of the RTD. Here,
305 three tests concerning the unsaturated zone (UZ) are presented, as this uncertainty accounts
306 for the strongest error source in the calculation. The parametric tests presented will focus on
307 the UZ profiles spatialisation. Three models are presented in the Results section:

1. RTD_T1: For this scenario, it was considered that the UZ consisted of only one filtering facies of sand (Profile SD) and no vertical karstic conduits.
2. RTD_T2: This configuration corresponds to the results of the spatial analysis of the UZ profiles (best fit).
3. RTD_T3: This scenario uses the same hydrodynamic characteristics as T1 but adds 34 vertical karstic conduits, positioned according to the karstic network and a database cavity, assuming that not all the vertical conduits are necessarily known.

4. Results

4.1. Equivalent Peclet numbers and average residence times

The spatial distributions of the hydrodynamic parameters used for the calculation of the equivalent parameters and the intermediate calculations for RTD are presented in Fig. 2B. The data concern the four types of profiles (Table1) and the limestone karst aquifer layer in the saturated zone. The alluvium aquifer located above the limestone aquifer is not shown in Fig. 2B but was nevertheless taken into account in the calculation of the equivalent parameters. The Fig. 2B and C shows the spatialized values (V_d, L, θ, n_e and α) from the UZ and SZ layers. The second column gives the equivalent parameters (average residence times and equivalent Peclet numbers) for the n flow nets starting from the n grid cells and determined by equations 10 and 12.

4.2. RTD Calculations

The time discretization unit selected for contamimant transport was one month. This is consistent with the assumption of steady-state conditions for the hydrology.

Fig. 2D shows the residence time distribution calculated from equation 13. The three scenarios illustrate the variability of the results when parameters are varied in the unsaturated zone. The parameters described in Table 1 correspond to the RTD_2 scenario. In this highly karstified area, the residence times are short, less than 12 months, and the average residence time is

about 2 - 4 months. The two extreme cases (Fig. 3) show that the intensity of the concentration peak can be twice as high in a karstic system compared to sand.

4.3. Concentration calculated at the water borehole by the RTD model

Figure 4 shows the concentration at the water borehole calculated by the RTD model. The average flow reproduces the maximum groundwater concentrations in atrazine at the borehole. The Nash-Sutcliffe coefficient was determined for the period 1990 to 2005. The value reaches 0.70.

4.4. Vulnerability and risk mapping

A vulnerability map can be computed, considering that each flow net receives a contaminant mass M=1. The vulnerability can be estimated by prioritizing all the calculated RTDs (equation 16). Combining the vulnerability map with a hazard map (Fig. 2E) gives a risk map for atrazine in the watershed. The results obtained are scaled on a range from 0 to 100.

Compared to traditional vulnerability mapping, this approach adds the notion of hydraulic distance to from the borehole. Surfaces with a high index (in red) are not spatially the closest to the borehole.

5.Discussion

The Nash-Sutcliffe coefficient suggests that the implementation of the equations, the parameterization and the strong hypothesis proposed in the RTD model seem acceptable for a risk assessment approach.

Concerning the mass of Atrazine applied on the field, the survey and the coefficient used to evaluate the loss in organic soil give results in terms of water concentration at the

borehole in the same order of magnitude as the concentrations observed. The range of uncertainty on the discharge (Q) and on Atrazine input (M) means that one can compensate the other, and with the given data, it is difficult to determine where the greatest source of error in our calculation lies. The uncertainty on the vertical conduit location is a key parameter for a relevant vulnerability assessment.

The range of equivalent Peclet numbers and average residence times found for this aquifer is wide. That is why a karst system was chosen to test this model.

The hydrology was assumed to be steady state. Although many authors point out that water exchange between conduits and the surrounding rock drives the water quality at the karstic outlet (Charmoille et al., 2009), this strong hypothesis was made for large time steps, such as months or years. In these conditions, it is preferable to describe the average behaviour of the system, which is easier to use for risk assessment. High or low water stages can be estimated from the extreme discharge values (Fig.3).

Concerning the contaminant transport, the progressive decrease in atrazine concentration observed at the borehole is correctly described by the model and corresponds to the decrease in the quantites of atrazine applied to the maize crops (Table 1). The apparently erratic distribution of the atrazine concentrations observed is explained by the pulses of atrazine occurring 2 or 3 months after the injection periods. These results help to rationalize sampling campaigns and to ensure a better management of water resources.

No storage was observed and advective flow control was observed in this highly transitive system. However, a temporal shift of a few weeks (X axis) can be observed. The calculated concentrations appear before the observed ones. We hypothesize that the origin of this phenomenon is the uncertainty concerning the exact period of application. In our case, atrazine application was considered to occur once a year, in April, but in reality applications may have varied depending on the weather conditions.

The RTD model, based on literature datasets, made it possible to estimate a specific vulnerability, which can then be validated by field data. Fig. 2E can be validated by time series of contaminants observed in the water supply. There is no single solution that can fit the concentration time series at the borehole. While many spatial distributions can lead to the same lumped parameters, the advantage of the proposed approach is that it can test whether the working hypotheses are sustainable. This is an improvement over the usual method of vulnerability and risk assessment, and avoids the use of numerical groundwater flow models that are generally over-parametrized.

6. Conclusions

The specific vulnerability index locates the potential source of groundwater quality deterioration, but most assessment methods are qualitative. The Residence Time Distribution model can address temporal and transient aspects of contaminant spreading and represent them in a semi-quantitative manner. Such an approach makes it possible to establish a spatial risk or vulnerability indexes validated by water quality changes at the borehole. The dataset used in this method is commonly found in vulnerability studies. By using equivalent parameters to take the characteristics of each layer into consideration, the spatial complexity of the watershed can be reduced to an impulse response. The method based on the probability distribution of residence times is a semi-objective method that can help groundwater managers and decision-makers based on a physical approach to vulnerability assessment. The risk mapped with this methodology gives the opportunity to test the efficiency of land practice scenarios on the quality of the groundwater catchments.

Acknowledgements

This work is part of the PhD project supported by GEO-HYD (Antea members) and a national grant from the National Research and Technology Association (ANRT – CIFRE).

409 The database used was made available by the INSU/CNRS national observatory of karstic
410 aquifers, SNO KARST.
411

412 **References**

413 Albéric P (2004) River backflooding into a karst resurgence (Loiret, France). Journal of
414 Hydrology 286: 194-202.
415 Aller L, Bennett T, Lehr JH, Petty RJ, Hackett G (1987) DRASTIC: a standardized system for
416 evaluating groundwater pollution potential using hydrogeological settings. US
417 Environmental Protection Agency. Washington, DC, USA.
418 Andersen L, Gosk E (1987) Applicability of vulnerability maps: Vulnerability of soil and
419 groundwater to pollutants, Proceedings and Information. TNO Committee on Hydrological
420 Research 28: 321-332
421 Aris R (1959) On the dispersion of a solute by diffusion, convection and exchange between
422 phases. Chemical reaction Engineering, doi: A252
423 Auterives C, Binet S, Albéric P (2014) Inferred conduit network geometry from geological
424 evidences and water-head in a fluvio-karstic system (Val d'Orleans, France). Environment
425 Earth Sciences. doi: 10.1007/978-3-319-06139-9_3
426 Bakalowicz M (2005) Karst groundwater: a challenge for new resources. Hydrogeology Journal.
427 doi: 10.1007/s10040-004-0402-9
428 Barry DA, Parker JC (1987) Approximations for solute transport through porous media with flow
429 transverse to layering. Transport in porous media, 2: 65-82
430 BDAT-GISSOL-INRA (2014). *http://www.gissol.fr/programme/bdat/bdat.php*. Accessed 10
431 December 2014
432 Beltman WHJ, Boesten JJTI, Van der Zee SEATM (1994) Analytical modelling of pesticide
433 transport from the soil surface to a drinking water well. Journal of Hydrology 169: 209-228

434 Binet S, Motellica M, Touze S, Bru K, Klinka T (2014) Water and Acrylamide monomer transfer
435 rates from a settling basin to groundwaters. Environmental Science and Pollution Research.
436 doi: 10.1007/s001090000086
437 Brouyère S (2001) Modelling of dual porosity media: comparison of different techniques and
438 evaluation on the impact on plume transport simulations. PhD Thesis Liège University
439 Chéry J (1983) Etude hydrochimique d'un aquifère karstique alimenté par perte de cours d'eau
440 (La Loire): Le système des calcaires de Beauce sous le Val d'Orléans. PhD Thesis Orléans
441 University
442 Civita M, De Maio M (2004) Assessing and mapping groundwater vulnerability to contamination:
443 The Italian "combined" approach. Geofisica Internacional 4: 513-532
444 Charmoille A, Binet S, Bertrand C, Guglielmi Y, Mudry J (2009) Hydraulic interactions between
445 fractures and bedding planes in a carbonate aquifer studied by means of experimentally
446 induced water-table fluctuations Coaraze experimental site, southeastern France.
447 Hydrogeology journal 17: 1607-1616
448 Desprez N (1967) Inventaire et étude hydrogéologique du Val d'Orléans. Rapport BRGM D-
449 SGR-67-A21
450 Doerfliger N, Jeannin PY, Zwahlen F (1999) Water vulnerability assessment in karst
451 environments: a new method of defining protection areas using a multi-attribute approach
452 and GIS tools (EPIK method). Environmental Geology 39: 165-176
453 Escolero OA, Marin LE, Steinich B, Pacheco AJ, Cabrera SA, Alcocer J, (2002) Development
454 of a Protection Strategy of Karst Limestone Aquifers: The Merida Yucatan, Mexico Case
455 Study. Water Resour Manag 16: 351–367

456 Fernandez GP, Chescheir GM, Skaggs RW, Amatya DM (2006) DRAINMOD – GIS: A lumped
457 parameter watershed scale drainage and water quality model. Agricultural Water
458 Management. doi: 10.1016/j.agwat.2005.03.004
459 Flury M (1996) Experimental evidence of transport of pesticides through field soils - A review.
460 Journal of Environmental Quality 25: 25-45
461 Footways/Géo-Hyd (2013) Application Phyto'Scope au Val d'Orléans: Outils d'évaluation du
462 transfert des produits phytosanitaires de leurs zones d'application vers les eaux de surface et
463 les eaux souterraines
464 Gelhar LW (1992) A critical review of data on field-Scale Dispersion in Aquifers. Water
465 resources research 7: 1955-1974
466 Goldscheider N, Hötzl H, Fries W, Jordan P (2001) Validation of a vulnerability map (EPIK)
467 with tracer tests. 7th Conference on Limestone Hydrology and Fissured Media. Sci.Tech
468 Environ Mém. 13: 167-170
469 Goldscheider N, Popescu C (2003) Vulnerability and risk mapping for the protection of carbonate
470 (karst) aquifer. European commission Directorate - General for Research, pp 320
471 Gutierrez A, Binet S (2010) La Loire souterraine: circulations karstiques dans le Val d'Orléans.
472 Géosciences 12 : 42-53
473 Holman IP, Palmer RC, Bellamy PH, Hollis JM (2005) Validation of an intrinsic groundwater
474 pollution vulnerability methodology using a national nitrate database. Journal of Hydrology.
475 doi: 10.1007/s10040-005-0439-4
476 IUPAC (2013) Global availability of information on agrochemicals. University of Hertfordshire.
477 http://sitem.herts.ac.uk/aeru/footprint/es/Reports/43.htm. Accessed 10 April 2013

478 Jeannin PY, Cornaton F, Zwahlen F, & Perrochet P (2001) VULK: a tool for intrinsic
479 vulnerability assessment and validation. 7th Conference on Limestone. Hydrology and
480 Fissured Media, pp 185-190
481 Joigneaux E (2011) Etat qualitatif des eaux de la nappe du Val d'Orléans; Impact du changement
482 climatique et gestion durable de la ressource. PhD Thesis Orléans University
483 Joigneaux E, Albéric P, Pauwels H, Pagé C, Terray L, Bruand A (2011) Impact of climate change
484 on groundwater point discharge: backflooding of karstic springs (Loiret, France). Hydrol.
485 Earth Syst. Sci. 15: 2459-2470
486 Joodi AS, Sizaret S, Binet S, Bruand A, Alberic P, Lepiller M (2009) Development of a Darcy-
487 Brinkman model to simulate water flow and tracer transport in a heterogeneous karstic aquifer
488 (Val d'Orléans, France). Hydrogeology journal 18: 295-309

489 Jurgens BC, Böhlke JK, Eberts SM (2012) Tracer LPM (Version 1): An Excel ® workbook for
490 interpreting groundwater age distributions from environmental tracer data. US Geological
491 Survey Techniques and Methods Report 4-F3, USA
492 Jury A (1982) Simulation of solute transport using a transfer function model. Water Resources
493 Research 2: 363-368
494 Kladivko EJ, Van Scoyoc GE, Monke EJ, Oates KM, Pask W (1991) Pesticide and nutrient
495 movement into subsurface tile drains on a silt loam soil in Indiana. Journal of Environmental
496 Quality 20: 264-270
497 Kreft A, Zuber A (1978) On the physical meaning of the dispersion equation and its solutions for
498 different initial and boundary conditions. Chemical Engineering Science 33: 1471-1480
499 Larsbo M, Jarvis N (2003) A model of water flow and solute transport in macroporous soil.
500 Technical description. Studies in the biogeophysical Environment. Swedish

501 Lasserre F, Razack M, Banton O (1999) A GIS-linked model for the assessment of nitrate
502 contamination in groundwater. Journal of Hydrology 224: 81-90
503 Ledoux E (2003) Modèles mathématiques en hydrogéologie. Document du Centre d'Information
504 Géologique Ecole Nationale Supérieur des Mines de Paris, Paris
505 Lelong F, Jojza N (2008) Fonctionnement du système karstique du Val d'Orléans: les acquis, les
506 interrogations. CFH - Colloque hydrogéologie karst au travers des travaux de Michel
507 Lepiller, Orléans
508 Lepiller M (2006) Le Val d'Orléans. Aquifère et eaux souterraines en France (BRGM), pp
509 200-214
510 Levenspiel O (1962) Chemical reaction engineering. New York
511 Li C, Ren L (2011) Estimation of unsaturated soil hydraulic parameters using the ensemble
512 kalman filter. Vadoze Zone Journal 10: 1205-1227
513 Livrozet E (1984) Influence des apports de la Loire sur la qualité bactériologique et chimique de
514 l'aquifère karstique du Val d'Orléans. PhD Thesis Orléans University
515 Maloszewski P Zuber A (1982) Determining the turnover time of groundwater systems with the
516 aid of environmental tracers – 1. Models and their applicability. Journal of hydrology 57:
517 207-231
518 Martin JC, Noyer ML (2003) Caractérisation du risque d'inondation par remontée de nappe sur
519 le Val d'Orléans. BRGM, Orléans
520 Molénat J, Davy P, Gascuel-Odoux C, Durand P (1999) Study of three subsurface hydrologic
521 systems based on spectral and cross-spectral analysis of time series. Journal of Hydrology
522 222: 152-164
523 Nash JE, Sutcliffe JV (1970) River flow forecasting through conceptual models part I - A
524 discussion of principles. Journal of hydrology 10: 282-290

525 Neukum C, Hötzl H, Himmelsbach T (2008) Validation of vulnerability mapping methods by
526 field investigations and numerical modelling. Hydrogeology Journal. doi:10.1007/s10040-
527 007-0249-y
528 Panagopoulos GP, Antonakos AK, Lambrakis NJ (2006) Optimization of the DRASTIC method
529 for groundwater vulnerability assessment via the use of simple statistical methods and GIS.
530 Hydrogeology Journal 14: 894-911
531 Petelet-Giraud E, Doerfliger N, Crochet P (2001) RISKE: Méthode d'évaluation multicritère de
532 la cartographie de la vulnérabilité des aquifères karstiques. Application aux systèmes des
533 Fontanilles et Cent-Fonts (Hérault, France). Hydrogéologie 4: 71-88
534 Plummer R, de Loë R, Armitage D, (2012) A Systematic Review of Water Vulnerability
535 Assessment Tools. Water Resour. Manag. 26: 4327–4346
536 Sadek MA, Abd El-Samie SG (2001) Pollution vulnerability of the Quaternary aquifer near Cairo,
537 Egypt, as indicated by isotopes and hydrochemistry. Hydrogeology Journal. doi:
538 10.1007/s100400100125
539 Schwientek P, Maloszewski P, Einsiedl F (2009) Effect of the unsaturated zone thickness on the
540 distribution of water mean transit times in a porous aquifer. Journal of Hydrology 373:
541 516-526
542 Šimůnek J, Šejna M, Sakai M, Van Genuchten M Th. (2008) The HYDRUS-1D Software
543 Package for Simulating the One-Dimensional Movement of Water, Heat, and Multiple
544 Solutes in Variably-Saturated Media. Riverside, California
545 Srinivasan R, Arnold JG (1994) Integration of basin-scale water quality model with GIS. Water
546 resources 30: 453-462

547 Visser A, Dubus IG, Broes HP, Brouyère S, Korcz M, Orban P (2009) Comparison of methods
548 for the detection and extrapolation of trends in groundwater quality. Journal of
549 Environmental Monitoring. doi:10.1039/B905926A
550 Voltz M, Louchart X (2001) Les facteurs clés de transfert des produits phytosanitaires vers les
551 eaux de surface. Ingénieries - Phytosanitaires, pp 45-54
552 Vrba J, Zaporozec A (1994) Guidebook on Mapping Groundwater Vulnerability. USA
553 Wauchope RD (1978) The pesticide Content of Surface Water Draining from Agricultural Fields.
554 Journal of Environmental Quality 7: 459-472
555 Zwahlen F et al (2003) COST Action 620 - Vulnerability and risk mapping for the protection of
556 carbonate (karst) aquifers. Final Report. European Cooperation in the field of scientific and
557 technical research (COST Action 620)

558 **TABLE CAPTIONS**

	Velocity (Vd)	Water content (q)	Longitudinal dispersivity coefficient (αL)	Length of flow (L)
Units	[m/s]	[-]	[m]	[m]
Unsaturated profiles SD	$2.31.10^{-7}$	0.33	0.4	1.49 to 16.49
Unsaturated profiles SD/LM	$1.00.10^{-8}$	0.4	0.4	4.22 to 9.39
Unsaturated profiles SD/CL	$3.50.10^{-9}$	0.5	0.5	1.99 to 13.5
Unsaturated profiles CL/SD	$3.50.10^{-9}$	0.6	0.5	2.05 to 10.37
Saturated alluvium	9.10^{-8} to 6.10^{-4}	0.15	20	1 to 14467
Saturated limestone	8.10^{-8} to 2.10^{-2}	0.3	2.5	1 to 10139
Saturated kartic conduit	8.10^{-8} to 2.10^{-2}	1	38	1 to 10139
References	Li and Ren (2011), Joodi et al (2009)	Simunek et al. (2008)	Simunek et al. (2008) and Gelhar (1992), Binet et al. (2014)	Desprez, 1967

559

560 Table1: Hydrodynamic characteristics of the zone

561

562

563 **FIGURE CAPTIONS**

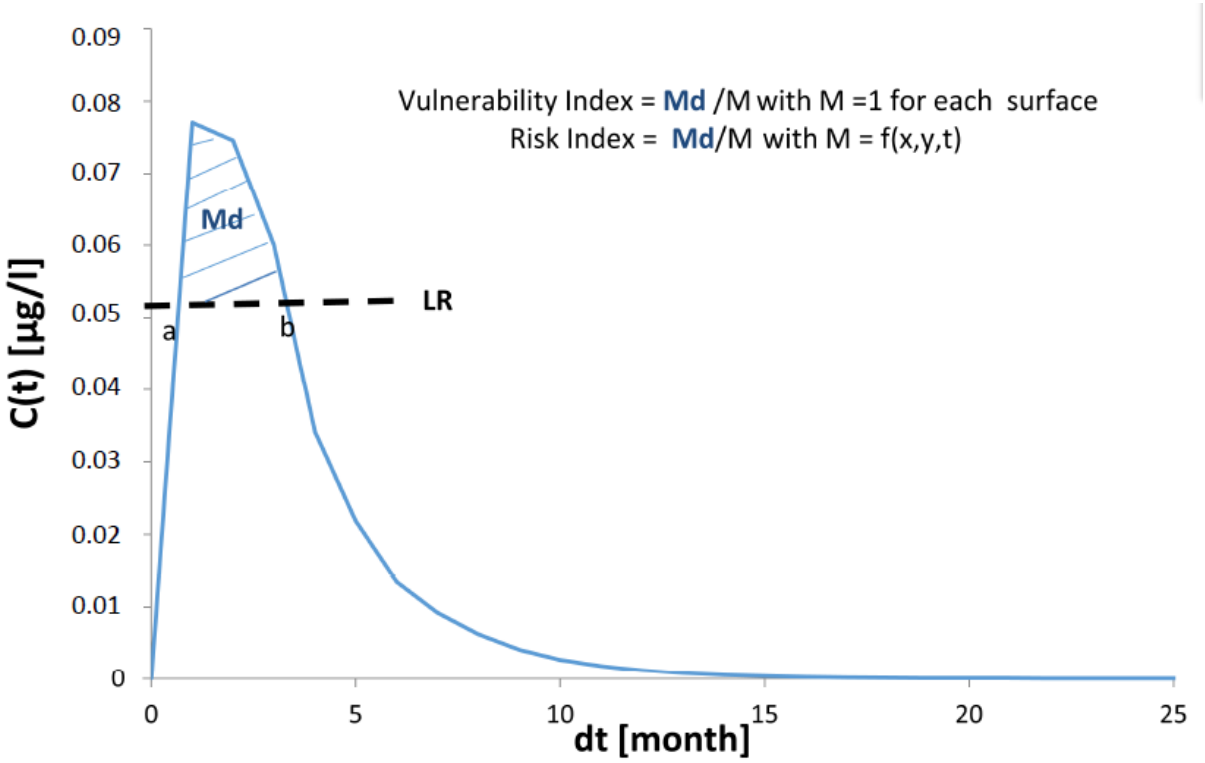

564

565 Fig. 1: Contaminant concentration versus time at the borehole, following a M=1 input for the
566 n^{th} flow net. Illustration of the relationship between the concept of vulnerability and the
567 R.T.D. curve: the vulnerability index can be defined as the “area under the curve” higher
568 than the fixed threshold (LR)

569

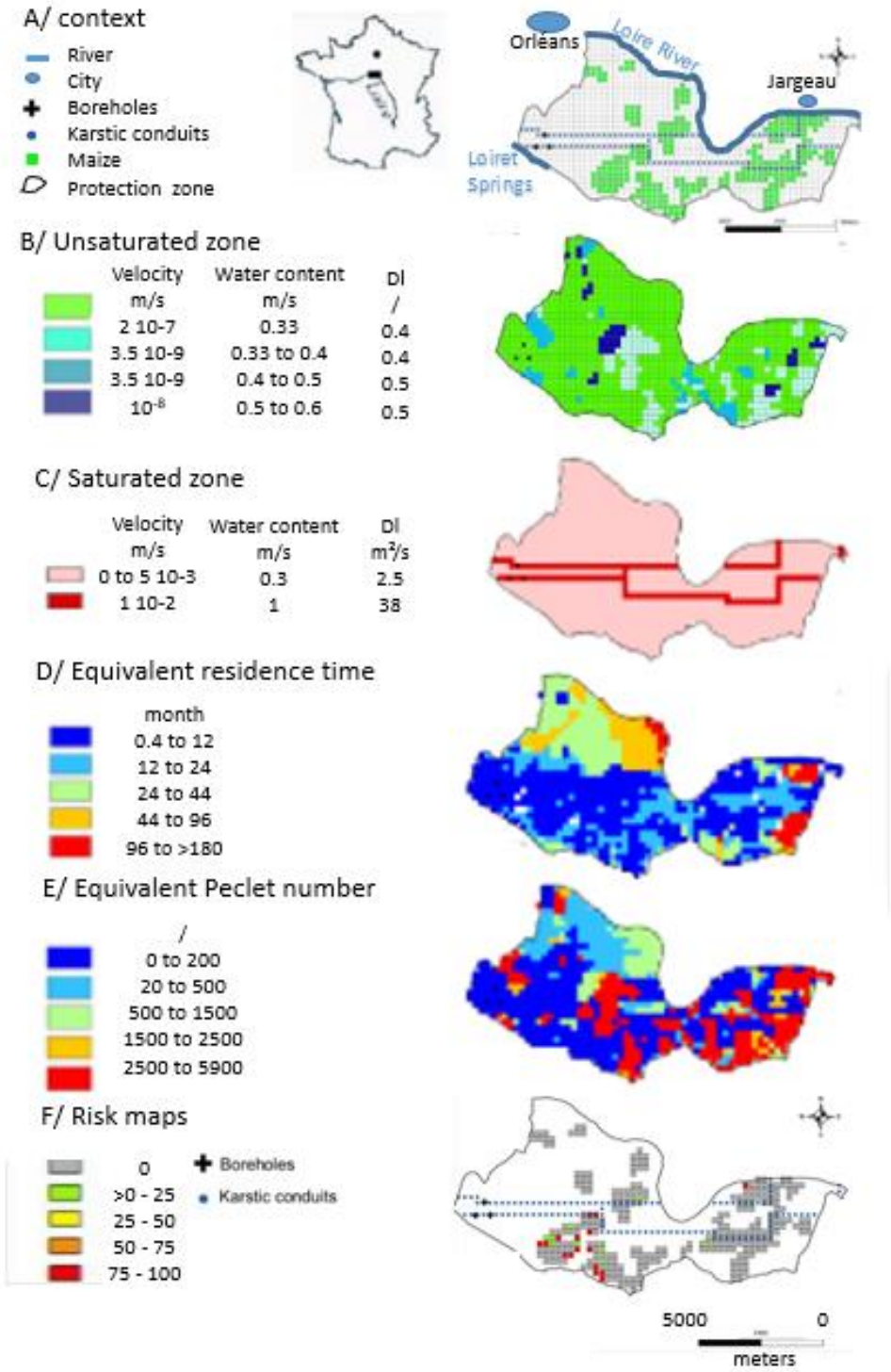

570

571 Fig. 2: The Val d'Orléans karstic aquifer, A/ grid discretization of the borehole watershed,
572 location of the 2010 maize crop. Spatial distribution of the parameters in B/ the
573 unsaturated and C/ saturated zones. D/ Equivalent residence time and E/ Peclet
574 number, F/ Specific risk map for Atrazine application in the borehole watershed.

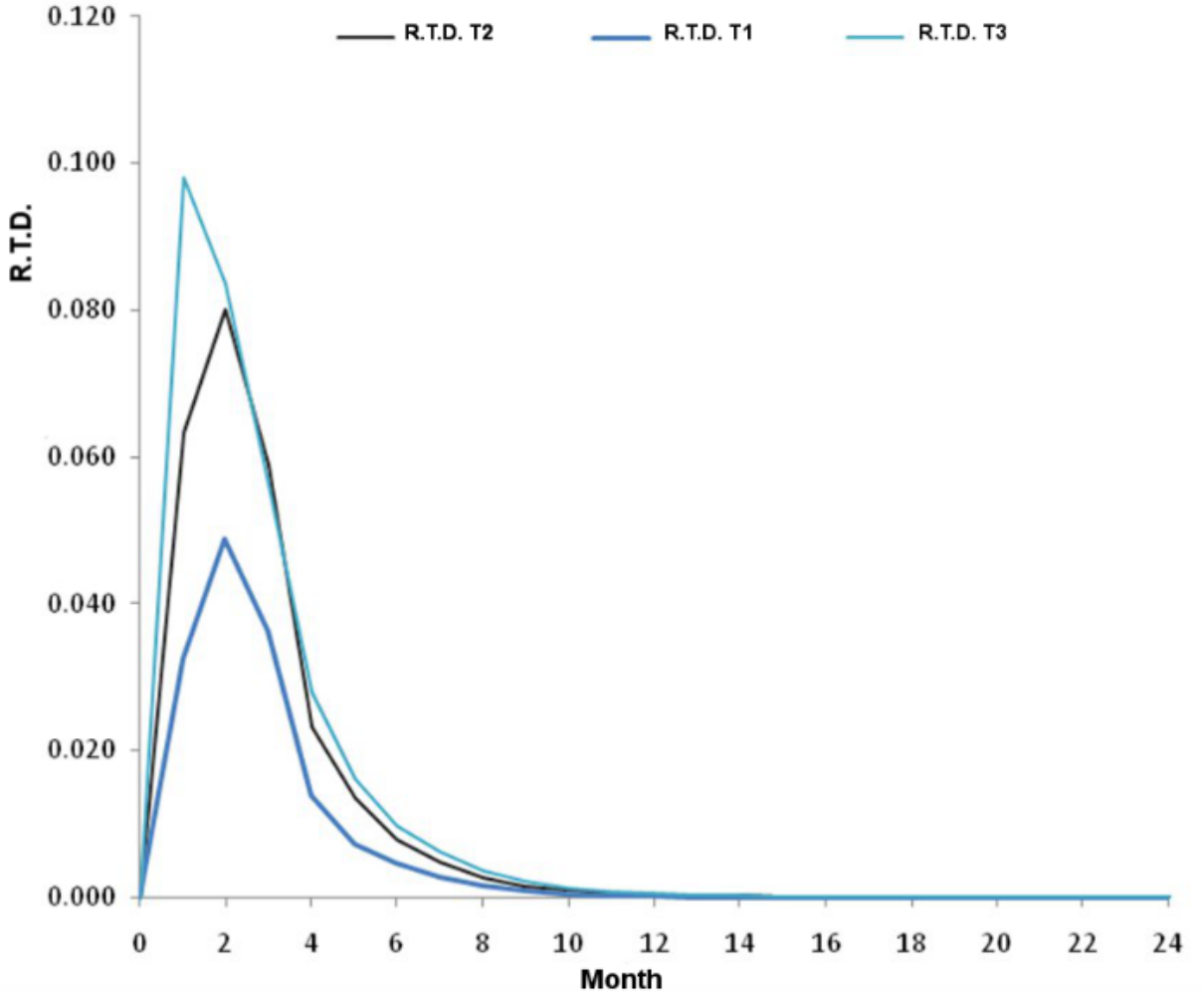

575

576 Fig. 3: R.T.D. variability for the Val d'Orléans borehole related to the properties of the
577 unsaturated zone. RTD T1: UZ profile is made of sand (SD), RTD T2 of sand (SD),
578 limestone (LM) and clay (CL), RTD T3 with sand (SD) and 34 karstic point recharges

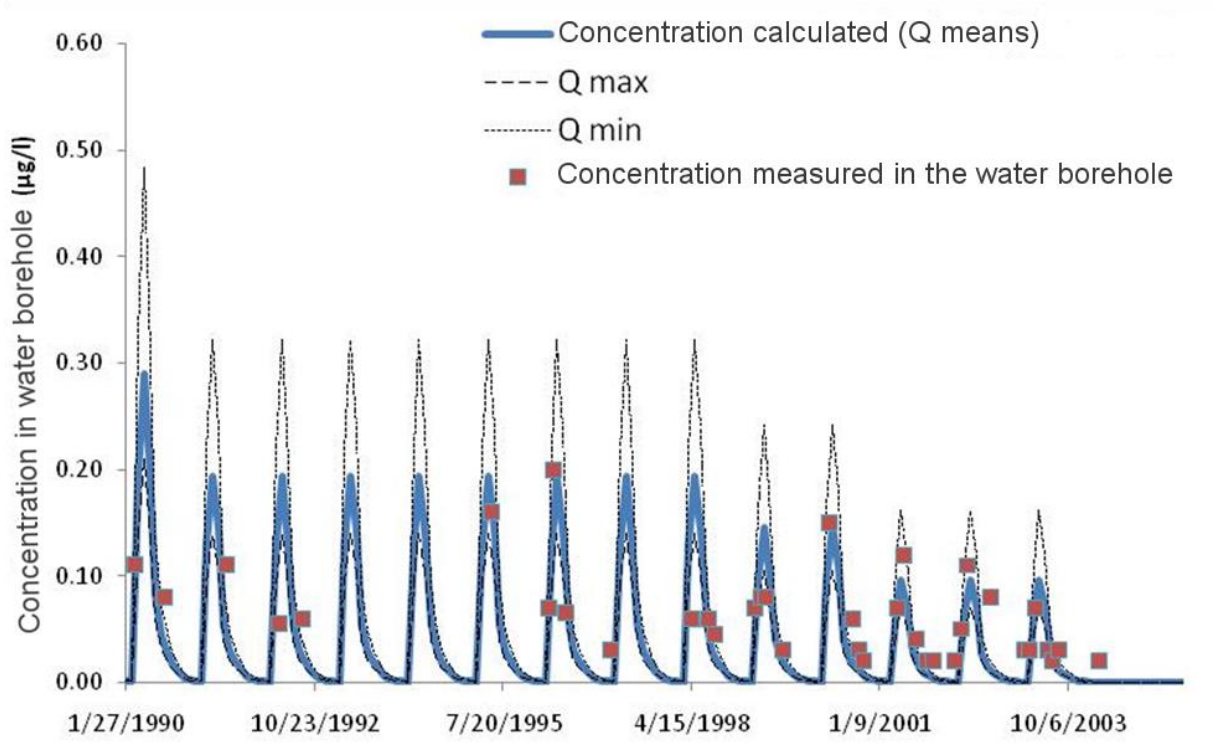

579

580 Fig. 4: Observed (crosses) and modeled (lines) atrazine concentrations versus time for high,

581 medium and low discharge values at the borehole

582